

# An analytic solution for the minimal bathtub toy model: challenges in the star-formation history of high- $z$ galaxies

Avishai Dekel<sup>1</sup>, Nir Mandelker<sup>1</sup>

<sup>1</sup>Center for Astrophysics and Planetary Science, Racah Institute of Physics, The Hebrew University, Jerusalem 91904 Israel; (dekel@huji.ac.il)

30 October 2018

## ABSTRACT

We study the minimal “bathtub” toy model as an analytic tool for capturing key processes of galaxy evolution and identifying robust successes and challenges in reproducing observations at high redshift. The source and sink terms of the continuity equations for gas and stars are expressed in simple terms from first principles. The assumed dependence of star-formation rate (SFR) on gas mass self-regulates the system into a unique asymptotic behavior, which is approximated by an analytic quasi-steady-state solution (QSS). We address the validity of the QSS at different epochs independent of earlier conditions. At high  $z$ , where the accretion is assumed to consist of gas only, the specific SFR is robustly predicted to be  $\text{sSFR} \simeq [(1+z)/3]^{5/2} \text{Gyr}^{-1}$ , slightly higher than the cosmological specific accretion rate, in agreement with observations at  $z = 3\text{--}8$ . The gas fraction is expected to decline slowly, and the observations constrain the SFR efficiency per dynamical time to  $\epsilon \simeq 0.02$ . The stellar-to-virial mass ratio  $f_{\text{sv}}$  is predicted to be constant in time, and the observed value requires an outflow mass-lading factor of  $\eta \simeq 1\text{--}3$ , depending on the penetration efficiency of gas into the galaxy. However, at  $z \sim 2$ , where stars are also accreted through mergers, the simplest model has an apparent difficulty in matching observations. The model that maximizes the sSFR, with the outflows fully recycled, falls short by a factor  $\sim 3$  in sSFR, and overestimates  $f_{\text{sv}}$ . With strong outflows, the model can reproduce the observed  $f_{\text{sv}}$  but at the expense of underestimating the sSFR by an order of magnitude. We discuss potential remedies including a bias due to the exclusion of quenched galaxies.

**Key words:** cosmology — galaxies: evolution — galaxies: formation — galaxies: kinematics and dynamics galaxies: spiral

## 1 INTRODUCTION

The bathtub toy model is simply the equation of conservation of gas mass in a galaxy, or in one of its components, sometimes combined with the analogous equation for stellar mass. The gas equation describes the net change of gas mass in the inter-stellar medium (ISM) as a difference between source terms and sink terms. When a whole galaxy is considered, the source term is the accretion rate, dictated by cosmology, but it can include recycled gas returning to the galaxy. The main sink terms are the rate at which gas turns into stellar mass and the gas outflow rate. The key for making the solution of this equation converge to a unique solution independent of the initial conditions is that the SFR is assumed to be proportional to the gas mass, and the other sink terms, especially the outflow rate, are assumed to be proportional to the SFR. This generates an interplay between the two components, where more

gas mass allows a higher SFR which in turn reduces the gas mass, thus driving the system into a self-regulated state that is determined by the relative efficiencies of accretion, SFR and outflows. When the accretion rate and the SFR timescale vary slowly enough, the asymptotic solution can be approximated by a quasi-steady state (QSS, sometimes termed “equilibrium”) that can be derived analytically.

The bathtub model is useful because it captures the key processes in a very simple and transparent way that makes it easy to trace their roles in the global evolution. It is appealing because it converges to a unique attractor solution, and even more so because of the analytic QSS solution. One of its attractive features is that at any time this solution is unique, independent of the initial conditions and independent of whether the same model was valid at earlier epochs. The model is thus useful even if its ingredients with specific values of the

model parameters are valid only in a relatively short cosmological time interval.

The bathtub model has become a very useful tool in understanding in simple terms the gross features of galaxy evolution. As summarized in Dekel et al. (2013), it has been applied in different ways to study different aspects of the the evolution of a whole galaxy (Bouché et al. 2010; Davé, Oppenheimer & Finlator 2011; Davé, Finlator & Oppenheimer 2012; Krumholz & Dekel 2012; Lilly et al. 2013; Birrer et al. 2014). Alternatively, it has been applied to the evolution of discs undergoing violent disk instability (VDI) where another sink term is the mass inflow from the disc to the central bulge (Dekel, Sari & Ceverino 2009; Cacciato, Dekel & Genel 2012; Genel, Dekel & Cacciato 2012; Forbes et al. 2013). Recently it has been applied to the mass evolution of individual giant clumps in VDI disks (Dekel, Bournaud & Mandelker 2014).

The bathtub toy model is not a replacement for the more elaborate semi-analytic models (SAMs) or for full hydro-cosmological simulations. This is a toy model, where on one hand the physical processes are represented by very idealized recipes but on the other hand their effects are fully transparent. It can thus serve for solid qualitative constraints on the parameters that characterize the accretion, SFR and outflows. It also serves for revealing robust successes or difficulties in understanding the origin of observed galaxy properties.

In the first part of this paper, we present the bathtub toy model and its ingredients in the case of a galaxy accreting from the cosmic web. We express the source and sink terms using the simplest possible scaling relations that we try to motivate from first principles rather than from simulations or observations. These simplified approximate expressions, in the Einstein-deSitter cosmological regime (approximately valid at  $z > 1$ ), allow an analytic derivation of the QSS solution. We numerically compute the asymptotic solution, derive the analytic QSS approximation, analyze its range of validity, and reveal the role played by each process in major observable quantities at different cosmological epochs.

In the second part we address three rather intriguing observational results at high redshift, which we describe in more detail in §5. First is the average specific star-formation rate (sSFR) for massive star-forming galaxies (SFGs) as a function of redshift, which current estimates show to decline from  $\sim 10 \text{ Gyr}^{-1}$  at  $z \sim 8$  through  $\sim 2 \text{ Gyr}^{-1}$  at  $z \sim 2$  to  $\sim 0.1 - 0.2 \text{ Gyr}^{-1}$  at  $z = 0$  (Whitaker et al. 2012; Stark et al. 2013; Labbé et al. 2013; Salmon et al. 2014). Second is the gas fraction in the galaxy,  $f_g$ , deduced to be  $\sim 0.5$  at  $z \sim 2$  and rather slowly declining with time at high redshifts (Daddi et al. 2010a; Tacconi et al. 2013). Third is the stellar-to-virial mass ratio,  $f_{sv}$ , estimated to be independent of redshift at  $z = 0 - 4$ , with a peak of  $\sim 0.025$  for halo masses in the range  $(0.5 - 5) \times 10^{12} M_\odot$  (e.g. Moster et al. 2010; Moster, Naab & White 2013; Behroozi, Wechsler & Conroy 2013, see §5). Given the universal baryon fraction  $f_b \simeq 0.17$ , this implies that only  $\sim 0.15$  of the baryons that were supposed to enter the halo have made it to the central galaxy. The sSFR that exceeds the ex-

pected specific accretion rate at all times, the high gas fraction as late as  $z \sim 2$ , and the very low  $f_{sv}$ , all pose non-trivial theoretical challenges.

In addition, the observed Kennicutt-Schmidt star-formation law (Kennicutt 1989), which can be interpreted as a relation between the SFR in a galaxy and its gas content, reveals a rather constant SFR efficiency in a free-fall time at the level of one to a few percent (Krumholz & Tan 2007; Krumholz & Thompson 2007; Daddi et al. 2010b; Genzel et al. 2010; Krumholz, Dekel & McKee 2012). Then, significant outflows are observed in high-redshift galaxies (Steidel et al. 2010; Genzel et al. 2011), with mass-loading factors ranging from below unity to 10. In both cases the uncertainties are large, so we prefer to treat these as free variables.

The paper is organized as follows. In §2 we present the bathtub model and its ingredients. In §3 we describe the quasi-steady-state solution and work out analytically observable quantities of interest. In §4 we study the validity of the QSS solution. In §5 we make a simple comparison of the model to observations. In §6 we discuss the successes and failures of the model in reproducing the observations, and address the assumptions made in the toy model. In §7 we conclude our findings concerning the toy model and the comparison to observations.

## 2 THE MINIMAL BATHTUB MODEL

### 2.1 Continuity Equations

The bathtub model consists of straightforward mass conservation for the gas mass  $M_g$  and the stellar mass  $M_s$  in an evolving galaxy,

$$\dot{M}_g = f_{ga} \dot{M}_a - (\mu + \eta) \dot{M}_{sf}, \quad (1)$$

$$\dot{M}_s = (1 - f_{ga}) \dot{M}_a + \mu \dot{M}_{sf}. \quad (2)$$

The accretion-rate term  $\dot{M}_a$  refers to *all* the baryons, gas and stars, as they *enter the galaxy for the first time*, where  $f_{ga}$  and  $f_{sa} = 1 - f_{ga}$  are the fractions of gas and stars in this accretion, respectively (to be spelled out in §2.2). The term  $\dot{M}_{sf}$  is the star-formation rate (SFR) (§2.3). The parameter  $\mu$  is the fraction of mass in forming stars that remains in stars, the rest assumed to be instantaneously lost from the stars due to supernovae and stellar winds and deposited back in  $M_g$  (Tinsley 1980), see §2.3. The parameter  $\eta$  is the *effective* mass-loading factor of the gas loss from the galaxy,

$$\eta = \frac{\dot{M}_{\text{loss}}}{\dot{M}_{sf}}, \quad (3)$$

referring to the net gas lost from the galaxy  $M_{\text{loss}} = M_a - M_b$ , where  $M_a$  is the total fresh baryonic mass accreted into the galaxy, and  $M_b = M_g + M_s$  is the baryonic mass in the galaxy. In our definition of the effective  $\eta$ , the mass loss is the outflow driven by stellar or AGN feedback minus the gas that flew out earlier and is now returning into the galaxy, termed “recycling” (§2.4).

## 2.2 Accretion Rate

The average specific accretion rate (sAR) of baryons into the galaxy,  $\dot{M}_a/M_a$ , is approximated by the specific accretion rate of total matter into the virial radius of the dark-matter halo,  $\dot{M}_v/M_v$ , where  $M_v$  is the total virial mass. The latter has been estimated quite robustly using theoretical considerations, confirmed and fine-tuned by simulations (Neistein & Dekel 2008). The estimate, based on very simple arguments in the EdS regime, gives (Dekel et al. 2013)

$$\frac{\dot{M}_a}{M_a} \simeq s(1+z)^{5/2} \text{Gyr}^{-1}, \quad s \simeq 0.03 \text{Gyr}^{-1}. \quad (4)$$

The power 5/2 is exact in the EdS regime, stemming from the fact that  $w \propto (1+z) \propto t^{-2/3}$  is a self-invariant time variable for structure formation, namely the halo-mass growth rate  $dM_v/dw$  is constant in time, so  $\dot{M}_v \propto \dot{w}$  with  $\dot{w} \propto t^{-5/3} \propto (1+z)^{5/2}$ . The slightly smaller powers proposed elsewhere (e.g. 2.2-2.4 proposed in Neistein, van den Bosch & Dekel 2006; Neistein & Dekel 2008) meant to provide global best fits in a larger redshift range, including the acceleration phase at  $z < 1$ . Similar fitting formulae based on simulations were proposed by others (Fakhouri & Ma 2008; Genel et al. 2008, 2010).

The approximation in eq. (4) ignores a weak additional mass dependence, roughly proportional to  $M_a^{0.14}$  (Neistein & Dekel 2008). The power 0.14, which fits simulations for  $M_v$  in the range  $10^{11} - 10^{14} M_\odot$ , originates from  $(n+3)/6$  where  $n \sim -2.1$  is the log slope of the linear fluctuation power spectrum on the relevant scales. By ignoring this weak mass dependence one does not introduce a large error as long as the analysis involves a mass range limited to one or two decades. This approximation is adopted in our minimal toy model for two important reasons, as follows.

First, having the specific accretion rate independent of mass makes the sAR adopted in eq. (4) the same at the halo virial radius and at the galaxy boundary in the inner halo. We assume that the fraction of the baryons in the total mass accreted (including dark matter) into the virial radius equals the universal baryonic fraction  $f_b \simeq 0.17$ . We denote by a *penetration* factor  $p$  the fraction of the baryons accreted into the virial radius that actually penetrate through the halo into the central galaxy,

$$p = \frac{M_a}{f_b M_v}. \quad (5)$$

The sAR is independent of  $p$  because both  $\dot{M}_a$  and  $M_a$  are proportional to the same  $p$ . The above is confirmed in hydro-cosmological simulations (Dekel et al. 2013, Figures 5 and 10), where  $p$  is found to be about 0.5. Thus, the minimal toy model with eq. (4) is independent of the actual value of  $p$ . However,  $p$  will enter when we compare the model predictions to the observed stellar-to-virial ratio that involves  $M_v$ .

The second benefit of the simple form of eq. (4) is that it can be integrated analytically to give a total

baryon mass growth (ignoring outflows) of

$$M_a = M_{ai} e^{-\alpha(z-z_i)}, \quad \alpha = 1.5 s t_1 = 0.79, \quad (6)$$

where  $M_{ai}$  is the initial value at time  $t_i$  or redshift  $z_i$ . Here we used the EdS approximation at  $z > 1$  (Dekel et al. 2013),

$$(1+z) = (t/t_1)^{-2/3}, \quad t_1 = 17.5 \text{Gyr}. \quad (7)$$

At very high redshift, and for galaxies with relatively low masses, one may assume in eq. (1)  $f_{ga} = 1$ . This has been the implicit assumption in several other applications of the bathtub model (e.g. Bouché et al. 2010; Davé, Finlator & Oppenheimer 2012; Lilly et al. 2013). However, by  $z \sim 2$  and for massive galaxies, there is a non-negligible fraction of ex-situ stars coming in through mergers,  $f_{sa} > 0$ . It will turn out below, as has already been noticed by Krumholz & Dekel (2012), that the value of  $f_{sa}$  makes a significant difference.

It may be helpful to compare our current notation with that of others who used the bathtub model, such as Davé, Finlator & Oppenheimer (2012, D12) and Lilly et al. (2013, L13). For example, our  $\mu$  is referred to in many cases as  $1 - R$ . Our penetration factor  $p$  is equivalent to  $\zeta$  of D12 (related to as ‘‘the preventive feedback parameter’’), and to  $f_{gal}$  of L13. In our case, however,  $p$  is not a basic parameter of the model. Our  $\varphi_s$  is the same as  $f_{star}$  in L12, so our stellar-to-virial mass ratio  $f_{sv} = p f_b \varphi_s$  is in their notation  $f_{gal} f_b f_{star}$ . The  $\dot{M}_{grav}$  of D12 is equivalent to our  $f_{ga} f_b \dot{M}_v = f_{ga} \dot{M}_a / p$ , and their  $\dot{M}_{prev}$  would be expressed in our notation as  $(1-p) f_{ga} f_b \dot{M}_v$ , where D12 and L13 implicitly assume  $f_{ga} = 1$ . The quantity  $\epsilon$  in L13 refers to the inverse of the depletion time,  $\text{SFR}/M_g$ , which in our notation is  $t_{sf}^{-1}$ , while in our notation  $\epsilon$  is the SFR efficiency in a dynamical time,  $\epsilon = t_d/t_{sf}$ , as more common in the literature. Our fiducial case assumes that our  $\epsilon$  is constant, while their fiducial case is with their  $\epsilon$  being constant. Finally, the modeling of recycling rate by D12 can be expressed as  $\dot{M}_{rec} = [\alpha_Z/(1-\alpha_Z)] \dot{M}_a$ , where  $\alpha_Z$  is the ratio of metallicities in the inflowing and ambient ISM gas. This is actually equivalent to the way we model recycling, except that they add it to the source term while we subtract it from the sink term, §2.4.

## 2.3 Star-Formation Rate

The key to a steady-state solution for eq. (1), motivated by the empirical Kennicutt-Schmidt law and theoretical considerations (e.g. Krumholz, Dekel & McKee 2012), is that the SFR is assumed to be proportional to the gas mass,

$$\dot{M}_{sf} = \frac{M_g}{t_{sf}}, \quad t_{sf} = \epsilon^{-1} t_d. \quad (8)$$

The time  $t_{sf}$  is the timescale for star formation to consume the gas reservoir (ignoring  $\mu$ ), also referred to as the *depletion* time (e.g. Genzel et al. 2008; Davé, Finlator & Oppenheimer 2012). We assume here that it is proportional to the disk dynamical crossing time

Quantity	Meaning	Definition	Fiducial value
$M_g, M_s$	gas, stellar mass in the galaxy		
$M_a$	baryon mass accreted onto the galaxy	eqs. (5) and (6)	
$\dot{M}_{\text{sf}}$	star-formation rate SFR	eq. (8)	
$\eta$	effective outflow mass-loading factor, $\eta = \eta_{\text{out}} - \eta_{\text{rec}}$	eqs. (3) and (10), §2.4	1
$\epsilon$	SFR efficiency per dynamical time	eq. (8)	0.02
$\mu$	fraction of stellar mass formed that remained in stars $\mu = 1 - R$	§2.1, §2.3	0.54
$s$	average specific accretion rate at $z = 0$ in $\text{Gyr}^{-1}$	eq. (4)	0.03
$f_b$	universal baryonic fraction	§2.2	0.17
$f_{\text{ga}}, f_{\text{sa}}$	gas, stellar fraction in the accretion	eqs. (1), (2)	1, 0 or 0.8, 0.2
$p$	penetration factor	eq. (5)	0.5
$A$	gas accretion rate $A = f_{\text{ga}} \dot{M}_a$	eq. (14)	
$t_d$	disc crossing time $R_d/V_d$	§2.3	
$\nu$	$t_d$ in units of the cosmological time	eq. (9)	0.0071
$t_{\text{sf}}$	star-formation or depletion time	eq. (8)	
$\tau$	$\tau = t_{\text{sf}}/(\mu + \eta)$	eq. (14)	
$f_g, f_s$	gas, stellar fraction of baryons in the galaxy	eq. (11)	
$\varphi_g, \varphi_s$	gas, stellar fraction of baryons accreted $M_a$	eq. (12)	
$f_{\text{sv}}$	stellar-to-virial mass ratio	eq. (13)	
sSFR	specific star-formation rate	eq. (22)	

**Table 1.** List of quantities and parameters

$t_d = R_d/V_d$ , where  $R_d$  and  $V_d$  are the characteristic radius and rotation velocity of the disc (Krumholz, Dekel & McKee 2012). As in Dekel et al. (2013), the disc dynamical time is approximated as proportional to the cosmological time,

$$t_d = \nu t, \quad \nu \simeq 0.0071. \quad (9)$$

We assume that the SFR efficiency factor per dynamical time  $\epsilon$  is constant over the time interval of interest and independent of galaxy mass in the mass range of interest. Its value is indicated to be on the order of 0.02 (e.g. Krumholz, Dekel & McKee 2012).

A value of  $\mu = 0.54$  has been estimated in Krumholz & Dekel (2012, Appendix A, where  $R = 1 - \mu$ ), adopting a Chabrier IMF and assuming that stars in the ranges  $(1 - 8)M_\odot$  and  $> 8M_\odot$  leave behind white dwarfs of  $0.7M_\odot$  and neutron stars of  $1.4M_\odot$  respectively. This estimate is valid after  $z \sim 2$ , where the age of the Universe is several Gyr. At higher redshifts, considering that only stars with lifetimes on the main sequence shorter than 3 Gyr (or 1 Gyr) had time to return mass to the ISM by  $z = 3$  (or  $z = 5.7$ ), one obtains  $\mu = 0.57$  (or 0.62). The maximum value relevant at very high redshifts is thus not very different from the value of 0.54 adopted throughout our current calculations.

## 2.4 Outflow and Recycling

The outflow rate due to stellar feedback,  $\dot{M}_{\text{out}}$ , is assumed to be proportional to the instantaneous SFR, with a constant mass-loading factor  $\eta_{\text{out}} = \dot{M}_{\text{out}}/\dot{M}_{\text{sf}}$ . Based on theory and observations of massive galaxies at  $z \sim 2$ ,  $\eta_{\text{out}}$  is expected to be of order unity or a few (Genzel et al. 2011; Dekel & Krumholz 2013).

A fraction of the gas that flew out at earlier times

is assumed to be returning at a recycling rate  $\dot{M}_{\text{rec}}$ . We crudely approximate this also to be proportional to the instantaneous SFR, with a corresponding constant factor  $\eta_{\text{rec}} = \dot{M}_{\text{rec}}/\dot{M}_{\text{sf}}$ . The effective mass-loading factor is

$$\eta = \eta_{\text{out}} - \eta_{\text{rec}}. \quad (10)$$

When recycling is taken into account, the effective  $\eta$  could be smaller than unity and even vanish.

In the quasi-steady-state solution discussed below (§3), the SFR becomes proportional to the gas accretion rate, eq. (21). In this case, the way we incorporate recycling becomes equivalent to assuming that it is proportional to the instantaneous accretion rate, and then adding the recycling to the source term instead of subtracting it from the sink term. The term to be added to the source term is  $\dot{M}_{\text{rec}} = [f_{\text{ga}}\eta_{\text{rec}}/(\mu + \eta)]\dot{M}_a$ .

## 2.5 Summary: Parameters and Observables

A summary of the model parameters is as follows. We adopt  $s = 0.03$ , the value estimated for the average sAR. We adopt  $\mu \simeq 0.54$  as a rather robust estimate at  $z < 2$ , and recall that it could be up to  $\sim 20\%$  higher at higher redshifts. The stellar fraction in the accretion,  $f_{\text{sa}}$ , will turn out to be rather important. It could be negligibly small at very high redshifts, say  $z \gtrsim 4$ , but it is likely to be non-zero at intermediate redshifts,  $z \sim 2$ . Once the parameters mentioned above are fixed at their fiducial values, the natural free parameters of the model are  $\epsilon$  and  $\eta$ , which could vary from below 0.01 to above 0.02, and from zero to more than a few, respectively. In the current simplest version of the bathtub model, we assume that all these parameters are mass independent in a certain relevant mass range, and are constant during a certain cosmological time interval.

The penetration parameter  $p$ , which is necessary only for the comparison with observed fractions that involve the virial mass and is not an intrinsic parameter of the model, could vary about a fiducial value of  $p \sim 0.5$ . This is based on hydro-cosmological simulations with a varying strength of supernova and momentum-driven feedback (Dekel et al. 2013, and work in preparation based on simulations with stronger feedback).

For convenience, we define dimensionless fractions as follows. The gas and stellar mass fractions with respect to the baryons in the galaxy are denoted

$$f_g = \frac{M_g}{M_b}, \quad f_s = \frac{M_s}{M_b}, \quad f_g + f_s = 1. \quad (11)$$

The corresponding fractions with respect to all the baryons accreted (including those that later flowed out) are

$$\varphi_g = \frac{M_g}{M_a}, \quad \varphi_s = \frac{M_s}{M_a}, \quad \varphi_b = \frac{M_b}{M_a}, \quad \varphi_g + \varphi_s = \varphi_b. \quad (12)$$

Most useful for characterizing the solution are the two fractions  $f_g$  and  $\varphi_s$ , both because each will turn out to be sensitive to a different parameter,  $\epsilon$  or  $\eta$  respectively, and because they can be related to observations. The gas fraction  $f_g$  is directly observable, and  $\varphi_s$  is related to the observable stellar-to-virial mass ratio via the penetration parameter  $p$ , eq. (5),

$$f_{sv} = \frac{M_s}{M_v} = p f_b \varphi_s. \quad (13)$$

Assuming initial values for  $f_g$  and  $\varphi_s$  at an initial redshift  $z_i$ , eqs. (1) and (2) can be integrated forward in time. The third and most useful quantity is the sSFR, which is robustly predicted, insensitive to the values of  $\epsilon$  and  $\eta$ , and is observable.

Most of the quantities and parameters used are listed for convenience in Table 1. It may be helpful to compare our current notation with that of others who used the bathtub model, such as Davé, Finlator & Oppenheimer (2012, D12) and Lilly et al. (2013, L13). For example, our  $\mu$  is referred to in many cases as  $1 - R$ . Our penetration factor  $p$  is equivalent to  $\zeta$  of D12 (related to as “the preventive feedback parameter”), and to  $f_{gal}$  of L13. In our case, however,  $p$  is not a basic parameter of the model. Our  $\varphi_s$  is the same as  $f_{star}$  in L12, so our stellar-to-virial mass ratio  $f_{sv} = p f_b \varphi_s$  is in their notation  $f_{gal} f_b f_{star}$ . The  $\dot{M}_{grav}$  of D12 is equivalent to our  $f_{ga} f_b \dot{M}_v = f_{ga} \dot{M}_a / p$ , and their  $\dot{M}_{prev}$  would be expressed in our notation as  $(1 - p) f_{ga} f_b \dot{M}_v$ , where D12 and L13 implicitly assume  $f_{ga} = 1$ . The quantity  $\epsilon$  in L13 refers to the inverse of the depletion time,  $SFR/M_g$ , which in our notation is  $t_{sf}^{-1}$ , while in our notation  $\epsilon$  is the SFR efficiency in a dynamical time,  $\epsilon = t_d / t_{sf}$ , as more common in the literature. Our fiducial case assumes that our  $\epsilon$  is constant, while their fiducial case is with their  $\epsilon$  being constant. Finally, the modeling of recycling rate by D12 can be expressed as  $\dot{M}_{rec} = [\alpha_Z / (1 - \alpha_Z)] \dot{M}_a$ , where  $\alpha_Z$  is the ratio of metallicities in the inflowing and ambient ISM gas. This is actually equivalent to the way we model recycling,

except that they add it to the source term while we subtract it from the sink term, §2.4.

### 3 QUASI-STEADY-STATE

Figure 1 shows in solid lines the exact numerical solution of eqs. (1) and (2) for the observable quantities, with the parameter choice  $f_{sa} = 0$  and  $\epsilon = 0.02$ , and with  $p = 0.5$  multiplying  $\varphi_s$ . Shown for  $\eta = 1$  are cases with different initial conditions (left), which converge to a unique asymptotic solution independent of the initial conditions. Also shown are solutions for different values of  $\eta = 0, 1, 3$  (right). We next analyze the convergence to the asymptotic solution and derive it analytically.

#### 3.1 Steady-State and Quasi-Steady-State

Eq. (1) for  $M_g(t)$  is of the form

$$\dot{M}_g = A - \tau^{-1} M_g, \quad (14)$$

where the parameters are the gas accretion rate,  $A = f_{ga} \dot{M}_a$ , and the characteristic timescale,  $\tau = t_{sf} / (\mu + \eta)$ . The negative  $M_g$  term drives the system into a unique attractor solution.

If  $A$  and  $\tau$  are both constant in time, there is a simple solution to this equation,

$$M_g(t) = A \tau (1 - e^{-t/\tau}), \quad \dot{M}_g = A e^{-t/\tau}, \quad (15)$$

for the initial condition  $M_g = 0$  at  $t = 0$ . For  $t \gg \tau$ , the transient component decays exponentially and the solution converges asymptotically to the steady-state (SS) solution

$$M_g = A \tau, \quad \dot{M}_g = 0. \quad (16)$$

This is a stable attractive solution to which the solution converges independent of the initial value of  $M_g$  because  $\dot{M}_g$  is a decreasing function of  $M_g$ .

In the cosmological case  $A$  and  $\tau$  are varying in time, but rather slowly. If the variation timescale is significantly longer than  $\tau$  (see §4), then one can approximate  $A$  and  $\tau$  as being constant during periods of order  $\tau$  in which  $M_g$  is evolving rapidly, and assume a temporary steady-state solution in the form of eq. (16). We thus approximate the asymptotic quasi-steady-state (QSS) solution at  $t \gg \tau$  by

$$M_g(t) = A(t) \tau(t) = \frac{f_{ga} t_{sf}(t)}{\mu + \eta} \dot{M}_a(t). \quad (17)$$

In the approximate QSS solution, eq. (1) reads

$$M_g(t) = \frac{\theta(t)}{(\mu + \eta)} M_a(t), \quad (18)$$

where

$$\theta(t) = f_{ga} \frac{t_{sf}(t)}{t_a(t)}, \quad t_a = \frac{M_a}{\dot{M}_a}. \quad (19)$$

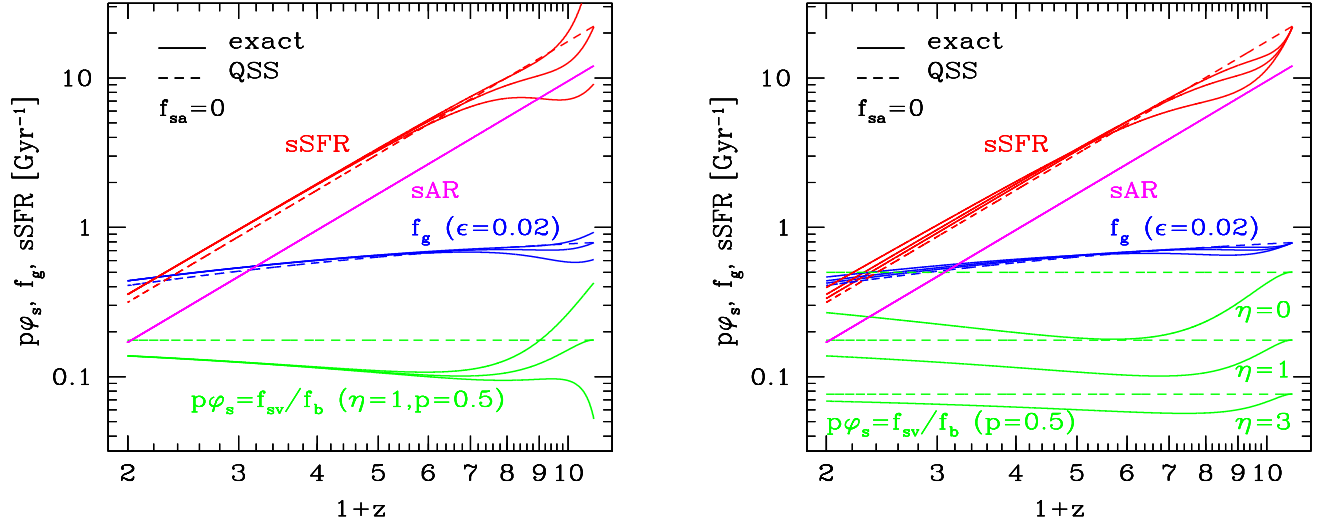


**Figure 1.** Solutions of the bathtub model as a function of  $1+z$ , representing time evolution from  $z_i = 10$  to  $z = 1$ . Shown are the exact solution (solid) and the QSS toy-model prediction (dashed). Shown are the sSFR (red) in comparison with the sAR, the gas fraction in the galaxy  $f_g$  (blue), and  $p\varphi_s$  with  $p = 0.5$  (green), which is the stellar-to-halo mass ratio divided by  $f_b = 0.17$ ,  $f_{sv}/f_b$ . The parameter choice here is  $f_{sa} = 0$  and  $\epsilon = 0.02$ , with  $\mu = 0.54$  and the average specific accretion rate (sAR, magenta) with  $s = 0.03 \text{ Gyr}^{-1}$ . **Left:** For  $\eta = 1$ , starting from three different initial conditions ( $C/M_{ai} = 0.5, 0, -0.25$ ) at  $z_i = 10$ . The exact solution converges to a unique asymptotic solution independent of the initial conditions on a timescale corresponding to  $\Delta z \sim 3$ . **Right:** For initial conditions that obey the QSS solution, and  $\eta = 0, 1, 3$  (top to bottom for the green curves, bottom up for the red and blue curves). The QSS solution reproduces the exact solution for  $f_g$  and sSFR very well. Its deviation from the exact model for  $\varphi_s$  (green) is consistent with eq. (35) – it is decreasing with time and with  $\eta$ .

According to eqs. (4), (9), and (7),  $\theta$  evolves as

$$\begin{aligned} \theta(t) &= f_{ga} s \nu t_1 \epsilon^{-1} (1+z) \\ &\simeq 0.186 f_{ga} s_{0.03} \epsilon_{0.02}^{-1} (1+z). \end{aligned} \quad (20)$$

According to the QSS solution, the SFR is proportional to the accretion rate,

$$\dot{M}_{sf} = \frac{f_{ga}}{\mu + \eta} \dot{M}_a. \quad (21)$$

### 3.2 QSS Solution for Observable Quantities

We next evaluate quantities of interest that also involve the stellar mass, using the QSS solution of eq. (1) combined with eq. (2). We focus on the observable quantities, (a) the gas fraction  $f_g$ , (b) the ratio of stellar mass to accreted baryon mass  $\varphi_s$  that is observable through the stellar-to-virial mass given by  $f_{sv} = p f_b \varphi_s$ , and (c) the specific SFR,

$$\text{sSFR} = \frac{\dot{M}_{sf}}{M_s}. \quad (22)$$

Inserting the QSS solution of eq. (1) into eq. (2), we obtain

$$\dot{M}_s = \frac{\mu + f_{sa} \eta}{\mu + \eta} \dot{M}_a. \quad (23)$$

If the parameters are all constant in time, and if the QSS solution is valid since an initial time  $t_i$ , one can integrate this equation in time to obtain

$$M_s(t) = \frac{\mu + f_{sa} \eta}{\mu + \eta} M_a(t) + C, \quad (24)$$

where  $C$  is the constant of integration, determined by the initial conditions at  $t_i$ . The choice  $C = 0$  is equivalent to

$$\varphi_b(t_i) = \frac{\theta(t_i) + \mu + f_{sa} \eta}{\mu + \eta}. \quad (25)$$

Even if  $C \neq 0$ , since  $M_a$  grows rapidly according to eq. (6), the role of  $C$  in eq. (24) becomes negligible a short while after  $z_i$ . For example,  $C/M_a$  drops by a factor of 10 by  $z - z_i \simeq -2.3/\alpha \simeq -2.9$ . Thus, the effect of the initial conditions on the solution for  $M_s$  is expected to become negligible after a time interval corresponding to  $\Delta z \sim 3$ , and the convergence is faster when the initial conditions do not deviate much from the asymptotic solution.

Adding the gas mass from eq. (17) and the stellar mass from eq. (24), the baryonic mass is

$$M_b(t) = \frac{\theta(t) + \mu + f_{sa} \eta}{\mu + \eta} M_a(t). \quad (26)$$

Then, from eqs. (17) and (26), the gas fraction is

$$f_g = \frac{\theta(t)}{\theta(t) + \mu + f_{sa} \eta}, \quad (27)$$

gradually decreasing with time following  $\theta(t)$ . Directly from eq. (24), we find that the stars-to-accreted-baryon fraction is constant in time,

$$\varphi_s = \frac{\mu + f_{sa} \eta}{\mu + \eta}, \quad (28)$$

and so is  $f_{sv} = p f_b \varphi_s$ . Finally, using eq. (21) and eq. (24), we find that the sSFR is proportional to the

specific accretion rate,

$$\text{sSFR} = \frac{\dot{M}_{\text{sf}}}{M_{\text{s}}} = \frac{f_{\text{ga}}}{\mu + f_{\text{sa}}\eta} \frac{\dot{M}_{\text{a}}(t)}{M_{\text{a}}(t)}, \quad (29)$$

namely, based on eq. (4),

$$\text{sSFR} = \frac{f_{\text{ga}}}{\mu + f_{\text{sa}}\eta} s_{0.03} (1+z)^{5/2} \text{Gyr}^{-1}. \quad (30)$$

For the case of gas accretion only,  $f_{\text{sa}} = 0$  ( $f_{\text{ga}} = 1$ ), which could be valid at very high redshift and for relatively small masses, the QSS expressions for the observable quantities reduce to

$$f_{\text{g}} = \frac{\theta(\epsilon; t)}{\theta(\epsilon; t) + \mu}, \quad \varphi_{\text{s}} = \frac{\mu}{\mu + \eta}, \quad \frac{\dot{M}_{\text{sf}}}{M_{\text{s}}} = \mu^{-1} \frac{\dot{M}_{\text{a}}}{M_{\text{a}}}. \quad (31)$$

It is a very interesting feature of this model, with  $f_{\text{sa}} = 0$ , that each of these observables is sensitive to another parameter of the model. Assuming that  $\mu$  is given, the gas fraction is determined by  $\epsilon$  through  $\theta$  and is independent of  $\eta$ . In contrast,  $\varphi_{\text{s}}$  depends on  $\eta$  only, so the observable  $f_{\text{sv}}$  depends on  $\eta$  and  $p$ . Most interestingly, the sSFR is independent of  $\epsilon$  and  $\eta$ ; its average is fixed by the rather robust estimates of  $\mu$  and  $s$ . This is a powerful prediction of this model.

Figure 1 shows in dashed lines the QSS solution, in comparison with the exact solution, for the same choices of parameters.

## 4 VALIDITY OF THE QSS SOLUTION

### 4.1 Error of the QSS Solution

We can estimate the error made by this approximation at time  $t$  as follows. The time derivative of the approximate  $M_{\text{g}}(t)$  from eq. (17) is  $\dot{M}_{\text{g}} = d(A\tau)/dt$ , instead of the  $\dot{M}_{\text{g}} = 0$  obtained when  $M_{\text{g}}$  from eq. (16) is inserted in the right-hand side of eq. (14). Based on this inconsistency, the error in  $\dot{M}_{\text{g}}$  can be estimated by  $\Delta\dot{M}_{\text{g}} = d(A\tau)/dt$ . Then, from eq. (14), with  $A$  given, the error in  $M_{\text{g}}$  is  $\Delta M_{\text{g}} = -\tau\Delta\dot{M}_{\text{g}}$ . Dividing this by the approximate  $M_{\text{g}}$  from eq. (17) one obtains

$$\frac{\Delta M_{\text{g}}}{M_{\text{g}}} \simeq - \left( \frac{\dot{A}}{A} \tau + \dot{\tau} \right). \quad (32)$$

The two terms correspond to the ratios of  $\tau$  and the timescales for variation in  $A$  and in  $\tau$ , respectively, which are the two quantities that were assumed to be small for the validity of the QSS.

For the time dependences of  $A(t)$  and  $\tau(t)$  assumed in our modeling above, we have from eq. (8)

$$\tau = \frac{t_{\text{sf}}}{(\mu + \eta)} = \frac{\epsilon^{-1\nu}}{(\mu + \eta)} t, \quad (33)$$

namely  $\tau \propto t$  and  $\dot{\tau} = \tau/t$ . From eq. (4) and eq. (6) we derive

$$\frac{\dot{A}}{A} t = \frac{2}{3} \alpha (1+z) - \frac{5}{3}. \quad (34)$$

These give in eq. (32)

$$\begin{aligned} \frac{\Delta M_{\text{g}}}{M_{\text{g}}} &\simeq -\frac{2}{3} \frac{\tau}{t} [\alpha(1+z) - 1] \\ &\simeq -\frac{0.236}{\epsilon_{0.02} (\mu + \eta)} [0.79(1+z) - 1]. \end{aligned} \quad (35)$$

For example, with  $\epsilon = 0.02$  and  $\eta = 2$ , the error in  $M_{\text{g}}$  is 5%, 13%, 27%, 57% at  $z = 1, 2, 4, 8$  respectively. Thus, the QSS solution is a better approximation at later times. This is despite the fact that according to eq. (33)  $\tau/t$  is the same at all times. The improvement with time is due to the fact that the timescale for variation of  $M_{\text{a}}$  with respect to  $t$  or  $\tau$  [namely  $(A/\dot{A})/\tau$ ] becomes longer in time. Note that the error associated with the QSS solution depends on all the model parameters, and, in particular, it is a decreasing function of  $\eta$ .

The relative errors in the SFR,  $M_{\text{s}}$  and  $M_{\text{b}}$  are expected to be comparable to the relative error in  $M_{\text{g}}$ . The error in  $\varphi_{\text{g}}$ ,  $\varphi_{\text{s}}$  and  $\varphi_{\text{b}}$  are therefore all expected to be comparable, and estimated by eq. (35), because  $M_{\text{a}}$  is given with no error. On the other hand, the errors in  $f_{\text{g}}$  and  $f_{\text{s}}$ , as well as in the sSFR, are expected to be of higher order and much smaller, because the errors in the numerators and in the denominators are similar and correlated.

Figure 1 shows that, once the transient components decay, the exact solution also approaches a unique asymptotic solution, independent of the initial conditions. The exact solution for  $\varphi_{\text{s}}$  deviates from the approximate QSS solution due to the time variation of  $A$  (and  $\tau$ ) following the error estimate in eq. (35). This deviation gradually diminishes at later times. Figure 1 (right) shows how this deviation depends on  $\eta$  – it is at the level of less than 25% for  $\eta = 3$ , 25-40% for  $\eta = 1$ , and a factor of 2 or more for  $\eta = 0$ . Even better than expected, the QSS solution for  $f_{\text{g}}$  and for the sSFR almost coincides with the exact asymptotic solution, making the analytic QSS solution very powerful.

### 4.2 Decay of Transients

The decay of the transient component in the exact solution can be estimated from its decay in the SS solution, eq. (15), namely  $\propto \exp(-t/\tau)$ . According to eq. (33),  $t/\tau$  is time-independent,

$$\frac{t}{\tau} \simeq 2.82 \epsilon_{0.02} (\mu + \eta). \quad (36)$$

Thus, the asymptotic regime  $t \gg \tau$  is valid at all times as long as  $\epsilon$  and  $\eta$  are sufficiently large. An exponential decay of the transient component by an order of magnitude, namely  $t/\tau \simeq 2.3$ , requires  $\mu + \eta \geq 0.82 \epsilon_{0.02}^{-1}$ . For  $\epsilon \simeq 0.02$  this condition is obeyed for any sensible value of  $\eta$ , while for  $\epsilon \simeq 0.01$  it requires that  $\eta$  exceeds unity. Note that the validity of the SS solution,  $t \gg \tau$ , depends on  $\epsilon$  and  $\eta$ , but is independent of the accretion rate  $A$  (namely  $f_{\text{ga}} \dot{M}_{\text{a}}$ ).

As explained in §3.2, if the initial conditions significantly deviate from the QSS solution, the corresponding

transients in the solution for  $M_s$  are expected to decay as  $\exp(-\alpha\Delta z)$ . This is demonstrated in Fig. 1. Shown in the left panel are three cases with different values of  $C$  in the initial conditions at  $z_i = 10$ , specifically  $C/M_{\text{ai}} = -0.25, 0, +0.5$ . We see that the exact solution converges to its unique asymptotic solution by  $z \sim 6-7$ , i.e., the transients decay significantly during  $\Delta z \sim 3$ , as expected.

### 4.3 A Physical QSS Solution

Eq. (18) implies

$$\varphi_g = \frac{\theta}{\mu + \eta}. \quad (37)$$

Since  $\theta$  is decreasing with time, eq. (20),  $\varphi_g$  must also be decreasing with time. The by-definition requirement that  $\varphi_g \leq 1$  induces a constraint on  $\theta(t)$  for a given  $\eta$ ,

$$\theta(t) \leq \mu + \eta. \quad (38)$$

Since  $\theta$  is decreasing with  $t$ , this translates to a lower limit on the time where the QSS solution could provide a physical solution with  $\varphi_g \leq 1$ . The interpretation of this constraint is that prior to this time the available gas mass is insufficient for the SFR to catch up with the intense accretion rate. During this early period, the gas mass grows in time and the accretion rate gradually declines, until the SFR can catch up with the accretion rate and the QSS solution is approached. Using eq. (20), with  $\epsilon = 0.02$ , we see that for  $\eta = 1$  the QSS solution is physical in the range  $z \leq 7.3$ , and for  $\eta \geq 1.5$  it is physical for  $z \leq 9.7$ , namely in the whole relevant range. However, for  $\epsilon = 0.01$ , with  $\eta = 1$  the physical solution is limited to  $z \leq 4.2$ , but with  $\eta = 3$  it is valid in the whole range,  $z \leq 8.5$ . Note that this validity criterion depends on the parameters  $\epsilon$  and  $\eta$  as well as on  $f_{\text{ga}}$  and  $\dot{M}_a$ .

## 5 COMPARISON TO OBSERVATIONS

### 5.1 Observations

We address here three rather intriguing observational results at high redshifts, indicated as symbols in Fig. 2.

First is the average sSFR for massive galaxies as a function of redshift. This either applies to galaxies selected to have a fixed mass at different redshifts, or to have the same comoving number density, thus assumed to mimic an evolving sample of galaxies. At  $z \leq 2$ , the results are relatively reliable thanks to measurements of  $H_\alpha$  and deep far-IR data. The average sSFR declines in time from  $2-2.5 \text{ Gyr}^{-1}$  at  $z = 2$ , through  $\simeq 0.7 \text{ Gyr}^{-1}$  at  $z = 1$ , toward  $\sim 0.1-0.2 \text{ Gyr}^{-1}$  at  $z = 0$  (Whitaker et al. 2012; Reddy et al. 2012). The high sSFR at  $z \sim 2$  and its potential conflict with theory have been noticed (Daddi et al. 2007), and led to considerations of a top-heavy IMF as a possible remedy (Davé 2008).

At higher redshifts, the estimate of sSFR requires non-negligible modeling and assumptions. The uncertainties in the stellar population models, and especially

the tentative implementation of emission lines, makes the results subject to systematic uncertainties by a factor of 2 or more. Early results indicated an apparent ‘‘sSFR plateau’’, with a constant sSFR in the range  $z = 2-8$  (e.g. Stark et al. 2009; González et al. 2010; Labbé et al. 2010). Attempts to model this sSFR plateau revealed severe difficulties (Weinmann, Neistein & Dekel 2011), and Krumholz & Dekel (2012) showed that it requires a non-negligible fraction of stars in the accretion. However, recent estimates have corrected the observed behavior of the sSFR at high redshifts, now showing a continuous decline with time. The calibration of absolute levels is more uncertain, with estimates of  $\text{sSFR} \sim 10 \text{ Gyr}^{-1}$  at  $z = 7-8$  declining to  $\sim 2-3 \text{ Gyr}^{-1}$  at  $z \sim 3$  (Gonzalez et al. 2012; Stark et al. 2013; Labbé et al. 2013; Duncan et al. 2014). In particular, estimates based on SED-fitting, that incorporates effects of nebular line emission and considers both starburst and SMC-type dust attenuation curves, reveal absolute values on the lower side (Salmon et al. 2014). It is encouraging that the decline rate is not very different from the decline predicted for the specific accretion rate, but the fact that the observed sSFR is still at a somewhat higher amplitude is challenging.

The second observation is the gas fraction in the galaxy, which is deduced from CO observations to be  $\sim 0.5$  at  $z \sim 2$  and declining with time (Daddi et al. 2010a; Tacconi et al. 2010, 2013). Many simulations fail to reproduce such high gas fractions as late as  $z \sim 2$ , as star formation in these simulations tends to consume most of the gas earlier. However, systematic errors are possible due to the assumed CO-to-gas conversion (Narayanan, Bothwell & Davé 2012) and due to a potential selection bias toward gas-rich galaxies (Tacconi et al. 2013).

The third observation is the stellar-to-virial mass ratio, estimated from observations of stellar masses using abundance matching of dark-matter haloes from simulations (Guo et al. 2010; Moster et al. 2010; Moster, Naab & White 2013; Behroozi, Wechsler & Conroy 2013). As can be seen in Figure 3 of Behroozi, Wechsler & Conroy (2013), it turns out to be rather independent of redshift in the range  $z = 0-4$ , with a maximum value of  $f_{\text{sv}} \sim 0.025$ , obtained for halo masses of  $M_v \sim (0.5-5) \times 10^{12} M_\odot$ . Given the universal baryon fraction  $f_b \simeq 0.17$ , this implies that only  $\sim 15\%$  of the baryons that were supposed to enter the halo have made it into stars at the central galaxy, namely  $f_{\text{sv}}/f_b = p\varphi_s \simeq 0.15$ , which is a non-trivial challenge for the modeling. We tentatively adopt this low estimate, but one should mention that new determinations of stellar masses in bright central galaxies of clusters indicate that the stellar-to-virial ratio for very massive haloes at low redshift is actually higher than the earlier estimates, by a factor of 2-4 (Bernardi et al. 2013; Kravtsov, Vikhlinin & Meshcheryakov 2014). This raises the potential worry that the adopted  $f_{\text{sv}}$  is an underestimate also on the scales of interest here,  $\sim 10^{12} M_\odot$ , and at high redshifts.

Significant outflows are observed in high-redshift galaxies (Steidel et al. 2010; Genzel et al. 2011), with

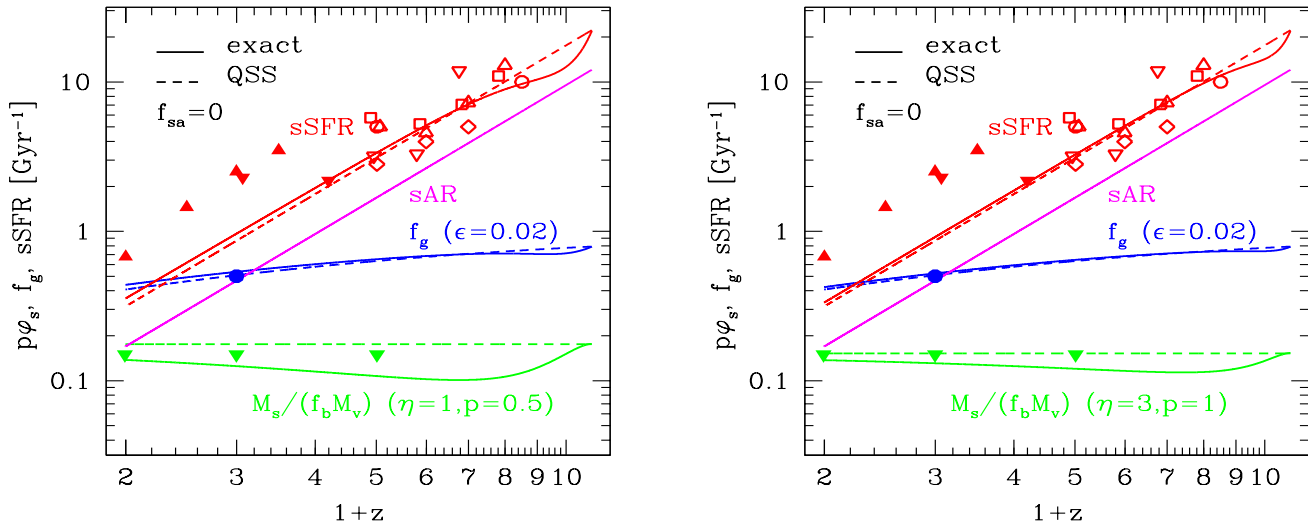


**Figure 2.** Solutions of the bathtub model with gas accretion only,  $f_{sa} = 0$ , with the average sAR, compared to observations. For more details see Fig. 1. Observational indications are marked by symbols. The sSFR measurements (red) are from Whitaker et al. (2012) (filled triangles), Reddy et al. (2012) (filled up-side-down triangles), Gonzalez et al. (2012) (up-side-down triangles), Labbé et al. (2013) (circles), Stark et al. (2013) (squares), Duncan et al. (2014) (triangles), Salmon et al. (2014) (diamonds). The gas fraction  $f_g$  at  $z \sim 2$  is from Tacconi et al. (2013) (blue circle). The stellar-to-virial mass ratio  $f_{sv}/f_b$  at  $z = 1 - 4$  is based on Behroozi, Wechsler & Conroy (2013) (green triangles). This bathtub model robustly reproduces the sSFR at  $z = 3 - 8$ , with  $\epsilon = 0.02$  uniquely constrained for matching the observed  $f_g$ . The value of  $\eta$  is constrained to be  $\eta = 1$  (left) or  $\eta = 3$  (right) for  $p\varphi_s$  to match the observed  $f_{sv}/f_b$  with a penetration factor of either  $p = 0.5$  or  $p = 1$  respectively. The only exception is the sSFR at  $z \sim 2$ , which is under-predicted by a factor of  $\sim 2 - 3$ .

a mass-loading factor ranging from below unity to 10, but the large uncertainty involved in these estimates makes us leave it as an open variable, to be determined by model fitting to the other observations. The situation is similar regarding the observed SFR efficiency (Krumholz & Tan 2007; Krumholz & Thompson 2007), which we leave free to be constrained by the other observations.

## 5.2 Gas Accretion Only

The simple QSS solution for the case of gas accretion only,  $f_{sa} = 0$ , is given in eq. (31). We can use it to evaluate the fit to the observed sSFR and estimate the best-fit values for  $\epsilon$  and  $\eta$ , which can then be fine-tuned using the exact solution. Figure 2 shows the observational constraints in comparison to the QSS and exact solutions with the best-fit choice of parameter values, as follows.

In order to obtain  $f_g \sim 0.5$  at  $z \simeq 2$ , one needs in eq. (31) a value of  $\theta \simeq 0.5$ , which, based on eq. (20), is obtained at  $z \simeq 2$  for  $\epsilon \simeq 0.02$ . Then, the value of  $f_g$  is predicted to be gradually larger at higher redshift, e.g.,  $f_g \sim 0.8$  at  $z \sim 10$ . A value of  $\epsilon \simeq 0.01$  gives at  $z = 2$  a gas fraction of  $f_g \simeq 0.67$ , which is too high, while  $\epsilon \simeq 0.04$  gives  $f_g \simeq 0.34$ , which is too low.

For the comparison with  $f_{sv}$  we assume a penetration of  $p = 0.5$ . In order to obtain the required low value for  $\varphi_s$  in eq. (31), one needs non-negligible outflows,  $\eta \sim 1$ . With  $p = 1$ , stronger outflows are required,  $\eta \sim 3$ . The solution for  $p\varphi_s$  is shown in Fig. 2 for  $p = 0.5$  and for  $p = 1$ . The fact that the exact solution for  $\varphi_s$  is lower than the corresponding QSS solution makes it

easier to match the low observed  $f_{sv}$  with somewhat lower values of  $\eta$ .

Finally, with  $\mu \simeq 0.54$ , the sSFR is roughly twice the specific accretion rate at all times in the QSS regime, independent of  $\epsilon$  or  $\eta$ . There is no choice of the model parameters that can give on average higher values of sSFR. The predicted values are  $\text{sSFR} = 0.94, 3.4, 7.8, 14.6 \text{ Gyr}^{-1}$  at  $z = 2, 4, 6, 8$  respectively. This is in good agreement with the observations at  $z = 3 - 8$ . However, at  $z \sim 2$ , the predicted average sSFR falls short by a factor of  $\sim 2$ . We will return to possible solutions to this puzzle in §6.2.

## 5.3 Including Stellar Accretion

With a non-vanishing value for the stellar fraction in the accretion,  $f_{sa}$ , the model faces difficulties in reproducing the observations. This is because the stellar accretion makes  $M_s$  grow without a corresponding growth in SFR, thus pushing the sSFR down and  $f_{sv}$  up (e.g., see the effect of a non-negligible  $f_{sa}\eta$  in the QSS solution, eq. (29) and eq. (28) respectively). Furthermore, with  $f_{sa} > 0$ , each of the observables becomes sensitive to more parameters than for  $f_{sa} = 0$ , and in particular the sSFR is pushed down, more so when  $\eta$  is larger. Also, the deviations of the QSS toy solution from the exact solution become larger, especially for the sSFR.

Figure 3 demonstrates these difficulties in the case  $f_{sa} = 0.2$ . The left panel refers to a low value of  $\eta = 0$ , trying to push the sSFR up as much as possible. A value of  $\eta \simeq 0$  may in fact have a sensible physical interpretation, where it represents a balance between outflow and recycling. A value of  $\epsilon = 0.015$  is now required for

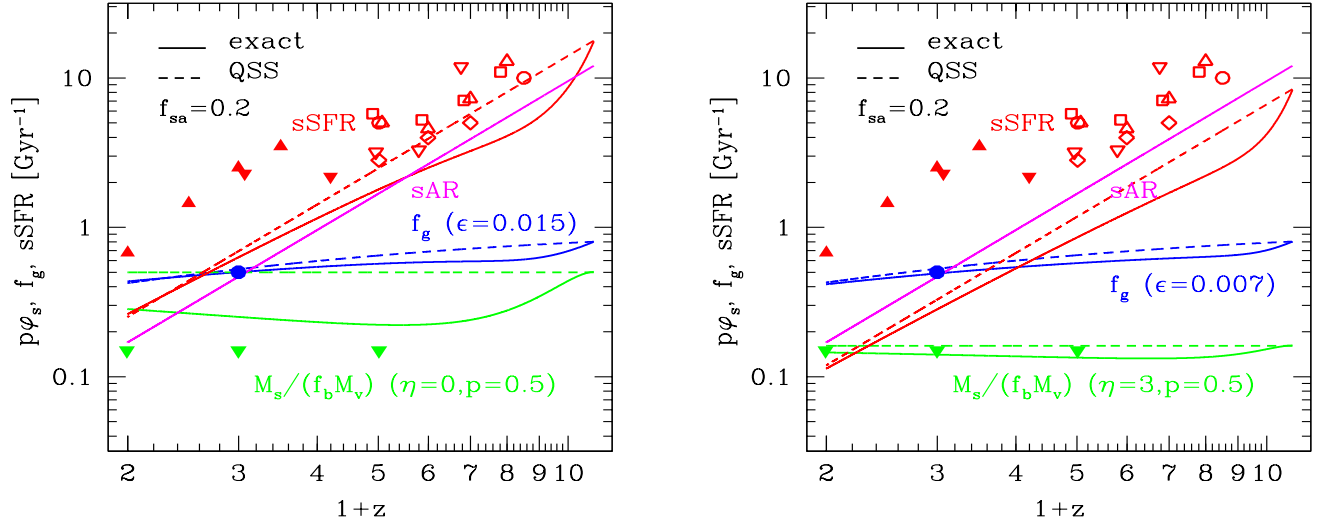


**Figure 3.** Solutions of the bathtub model including stellar accretion,  $f_{sa} = 0.2$ , with the average sAR, compared to observations. For more details see Fig. 1 and Fig. 2. **Left:** With maximum-recycling  $\eta = 0$  for maximum sSFR, and the best-fit  $\epsilon = 0.015$  for  $f_g$ . Even with this low  $\eta$  the sSFR is slightly under-predicted at  $z = 3 - 8$ , and by a factor of  $\sim 3$  at  $z = 2$ , while the  $f_{sv}/f_b$  is over-predicted by  $\sim 50\%$  even with  $p = 0.5$ . **Right:** With  $\eta = 3$  for a match of the  $f_{sv}/f_b$  with  $p = 0.5$ , and the best-fit  $\epsilon = 0.007$  for  $f_g$ . Now the sSFR is under-predicted by a factor of  $\sim 3$  at  $z = 3 - 8$ , and by a factor of  $\sim 7$  at  $z \sim 2$ .

a good match to  $f_g$  at  $z \sim 2$ , with no strong effect on the matching of the other observables. While the QSS solution is now a good match to the sSFR at  $z = 3 - 8$ , the exact solution slightly under-predicts the sSFR at  $z = 3 - 8$ , by  $\sim 30\%$ , and the predicted sSFR falls short more severely at  $z \sim 2$ , by a factor of  $\sim 3$ . With this low  $\eta$ , the exact solution for  $f_{sv}$  overestimates the observed value by  $\sim 50\%$  even with  $p = 0.5$ . If  $p = 1$ , the deviation from the observed value becomes a factor of  $\sim 3$ . One needs  $p \sim 0.3$  for a match. Note that the lowest possible value of  $\varphi_s$  is  $f_{sa}$ , obtained when  $\eta$  grows to infinity. Thus, a value of  $f_{sa} > 0.15/p$  will make it impossible to match the observed  $M_s/(f_b M_v) = 0.15$ .

The right panel of Fig. 3 appears to stronger outflows,  $\eta = 3$ , as required for a match of  $f_{sv}$  with  $p = 0.5$ . For this  $\eta$ , a value of  $\epsilon = 0.007$  provides the desired match to  $f_g$  at  $z \sim 2$ . However, now the failure in matching the sSFR becomes more severe – an under-prediction by a factor of  $\sim 3$  at  $z = 3 - 8$ , and by a factor of  $\sim 6 - 7$  at  $z \sim 2$

## 6 DISCUSSION

### 6.1 Model Fits Observations at $z = 3 - 8$

We should first recall that the asymptotic solution of the bathtub model with a given set of parameter values can be considered at a given cosmological period independent of whether it was valid at an earlier time.

At sufficiently high redshifts, and more so for less massive galaxies, the approximation of gas accretion only,  $f_{sa} = 0$ , may be naturally acceptable. In this case, the simplest possible bathtub toy model turned out to be extremely successful in qualitatively reproducing the observations, and in constraining the rates of star formation and outflows. The QSS solution naturally re-

produces the constancy in time of the stellar-to-virial mass ratio,  $\propto \varphi_s$ , and the gradual decrease of the sSFR with time at a level comparable and slightly higher than the theoretically estimated specific accretion rate. The observational requirement of  $f_g \sim 0.5$  soon after  $z \sim 3$  dictates an SFR efficiency in a disk dynamical time of  $\epsilon \sim 0.02$ , which is consistent with what we knew a priori (Krumholz & Tan 2007; Daddi et al. 2010b; Genzel et al. 2010). Independently, the requirement of  $p\varphi_s \sim 0.15$  dictates a mass-loading factor  $\eta \sim 1$  if the penetration is  $p \sim 0.5$ , as deduced from simulations (and  $\eta \sim 3$  if  $p \sim 1$ ). This is consistent with the observational indications for rather intense outflows (Steidel et al. 2010; Genzel et al. 2011). This toy model, and its analytic QSS solution, can thus be very useful in the interpretation of observations at very high redshifts, say  $z \geq 3$ .

However, at  $z \sim 2$ , and in massive galaxies, the stellar accretion via mergers is not likely to be negligible (Dekel et al. 2013). Even for  $f_{sa} \sim 0.2$ , and especially with non-negligible  $\eta$ , this component dominates the growth of stellar mass. It drives  $M_s$  up independent of the SFR, and thus pushes the sSFR down and  $\varphi_s$  up, away from the observed values. In this case, the model cannot simultaneously provide a perfect match to the high sSFR and the low  $\varphi_s$ , as the former favors vanishing effective outflows,  $\eta \ll 1$ , while the latter requires intense outflows,  $\eta \sim 3$ . The case  $\eta = 3$  is unacceptable, because the sSFR is severely under-predicted, by a factor of 3 at  $z = 3 - 8$  and by a factor of 7 at  $z \sim 2$ . The case  $\eta = 0$ , on the other hand, provides a potentially acceptable compromise, where the sSFR at  $z = 3 - 8$  is under-predicted by only 30% and  $f_{sv}$  is over-predicted by 50% for  $p = 0.5$ . The latter is properly matched if  $p = 0.3$ . Such a low value of  $p$  is possible since the haloes at  $z \sim 2$  and later are more likely to become more massive than the critical mass for virial shock

heating (Dekel & Birnboim 2006), where the penetration into the galaxy becomes more difficult. An alternative solution arises if the adopted low observed value of  $f_{\text{sv}}$  is an underestimate (as might be indicated by Kravtsov, Vikhlinin & Meshcheryakov 2014). An increase of  $\sim 50\%$  in the observed  $f_{\text{sv}}$  is needed for the model with  $\eta = 0$  to match it.

## 6.2 A Challenge at $z \sim 2$

The bathtub model highlights the fact that the sSFR at  $z \sim 2$  introduces a non-trivial challenge, with the observed value being  $\sim 3$  times the average specific accretion rate. Even for gas-accretion only, the predicted sSFR is short by a factor  $\sim 2$  compared to the observational estimates. With a relatively small component of stellar accretion,  $f_{\text{sa}} = 0.2$ , and with  $\eta = 0$ , the deviation becomes a factor of  $\sim 3$ . Higher values of  $f_{\text{sa}}$  or  $\eta$  would make this deviation more severe. Thus, matching the high sSFR at  $z \sim 2$  is not easy. We address possible solutions next.

### 6.2.1 Recycling

A potential explanation for the high sSFR at  $z \sim 2$  is recycling, the return of gas that has been ejected earlier by feedback but remained bound. Since gas is likely to accumulate in the galaxy at earlier periods when the SFR is low compared to the accretion rate, it may be available for strong outflows (especially in low-mass galaxies), to be followed by recycling into more massive galaxies at  $z \sim 2$ . The low SFR at very high redshifts may be due to the effect discussed in §4.3 where more gas is needed for the SFR to catch up with the intense accretion rate. It may also arise from a low SFR efficiency parameter  $\epsilon$ , e.g., due to low metallicity in the galaxy building blocks (Krumholz & Dekel 2012).

Recycling is modeled in our minimal bathtub model in a very crude way, as a negative contribution to  $\eta$ . The model with  $\eta = 0$  may thus be regarded as representing a period of intense recycling, where the return is at a rate comparable to the outflow rate at that time. With  $f_{\text{sa}} = 0.2$ , this brings the underprediction of the sSFR at  $z \sim 2$  to the level of a factor of  $\sim 3$ . The remaining deviation may possibly be reduced with a more sophisticated implementation of recycling in the modeling.

### 6.2.2 Other Parameters

One possibility for easing the tension concerning the sSFR at  $z \sim 2$  is to consider different average values for one or more of the model parameters. For example, the value of  $s$  describing the average sAR in eq. (4), deduced from simulations (e.g. Dekel et al. 2013), may possibly be an underestimate because the sample of galaxies simulated is biased against high-density environments, which are indeed more abundant at  $z \sim 2$  than earlier. A higher value of  $s$  would reproduce a higher sSFR, as desired.

Another possibility is that  $\mu$ , the fraction of star-forming mass that remains in stars, may actually be lower as a result of a top-heavy IMF. In this case one may wonder why this would happen at  $z \sim 2$  and not earlier.

### 6.2.3 Bias due to quenched galaxies

The high average sSFR indicated by observations at  $z \sim 2$  may reflect an observational selection bias toward the high sSFR galaxies, in the presence of scatter in the sSFR of different galaxies. Recall that galaxies are selected from the SFG population, which, by  $z \sim 2$ , constitute only about half the massive galaxies, the rest being already quenched by that time (e.g. Kriek et al. 2006; van Dokkum et al. 2008; Tal et al. 2014). A scatter can be introduced in the parameters of the bathtub model, that would lead to scatter in the predicted sSFR at a given time. However, our toy model does not attempt to model the actual quenching process, so the low-SFR galaxies are still star forming. The key for this effect to lead to a better agreement with the observed sSFR is that the sources for relatively low sSFR in the model would actually lead to an even lower sSFR, namely quenching, once quenching is incorporated, as in the real-Universe galaxies.

According to eq. (29), low sSFR is obtained in the model if  $s$  that characterizes the specific accretion rate in eq. (4) is low, and if  $\mu + f_{\text{sa}}\eta$  is high, namely when either  $\mu$  or  $f_{\text{sa}}\eta$  or both are high. We consider each of these sources of scatter. According to cosmological simulations, the distribution of  $s$  among snapshots, including scatter between galaxies and along the evolution of each galaxy, is  $\pm 0.45\text{dex}$  (Dekel et al. 2013, Figure 7). Based on hydro-cosmological simulations with supernova and radiative stellar feedback, we deduce a typical scatter of  $\pm 0.3\text{dex}$  in  $\eta$  and a similar scatter in  $f_{\text{sa}}$  among different output snapshots (House et al., in preparation; Tweed et al. in preparation). Scatter in  $\mu$  may reflect variations in the IMF.

High values of  $\eta$  and  $f_{\text{sa}}$  may indeed lead to quenching. A high  $\eta$  indicates gas removal by stellar or AGN feedback (with little recycling) that would naturally lead to quenching. A high  $f_{\text{sa}}$  is associated with a high dry-merger rate, which tends to occur in galaxy cluster environments, namely in more massive dark halos. Such halos are likely to be more massive than the critical mass for virial shock heating,  $\sim 10^{12}M_{\odot}$ , and thus likely to be subject to halo-mass quenching (Dekel & Birnboim 2006; Woo et al. 2013; Dekel & Burkert 2014). A low sSFR could occur in particular in a galaxy that is observed in a quiet accretion period but had significant gas-poor merging in the recent past, such that  $M_s$  grew significantly but the SFR is similar to what it was before the mergers. In such a post-merger galaxy, which could also be post-starburst and post-outflow, quenching follows by gas consumption and removal. As for low values of  $s$  or high values of  $\mu$ , while it is clear that they lead to low sSFR in the model, it is not clear whether they would lead to quenching in real galaxies.

### 6.2.4 Breakdown of the QSS

Another possible solution to the discrepancy at  $z \sim 2$  is a breakdown of the validity of the QSS solution over a short period of cosmological time. This could result from strong fluctuations in the gas accretion rate  $A$  with a short timescale, or similar fluctuations in the characteristic timescale  $\tau$ . Such fluctuations may invalidate the QSS and limit the usefulness of the bathtub model for describing the instantaneous properties of galaxies, while it may still trace the long-term average properties. For example, the sSFR may get temporarily high without a corresponding increase in  $M_s$  as a result of a star burst or a recycling burst.

### 6.3 Validity of the Model Assumptions

The ingredients of the minimal bathtub toy model discussed here involve certain simplifying assumptions worth discussing concerning the cosmology, accretion rate, SFR and outflows.

We have applied the model in the EdS regime,  $z > 1$ , in order to allow a simple analytic solution. However, the model can be easily applied in the regime where the  $\Lambda$ CDM cosmology deviates from the EdS approximation, down to  $z = 0$ . In this regime, the accretion rate deviates from the simple form of eq. (4), so the QSS solution has to be derived numerically. An extrapolation of the EdS expression to  $z = 0$  gives a value of sSFR below  $0.1 \text{ Gyr}^{-1}$ , already qualitatively consistent with observations, so it recovers much of the low-redshift decline without appealing to the acceleration of the Universe or to baryon-physics processes. Note that when plotting the sSFR as a function of  $z$  rather than  $\log(1+z)$ , the decline of the sSFR shows the familiar steepens with time after  $z \sim 2$ , following the associated drop in the sAR. The decline gets steeper when taking into account the acceleration of the Universe at  $z < 1$ , and the quenching of massive galaxies in shock-heated haloes at low redshifts (Dekel & Birnboim 2006; van de Voort et al. 2011). An extrapolation of the EdS solution to  $z = 0$  also yields a gas fraction estimate of  $f_g \sim 0.1$  (for  $\eta \sim 1$  and  $f_{sa} \sim 0.5$ , say), and a value of  $f_{sv}$  similar to its value at higher redshifts, both in the ballpark of the average observed values. The solution taking into account the acceleration phase is not very different.

A general limitation of the bathtub model is that the continuity equations refer to a given time, and the ingredients are all assumed to be instantaneous. In reality, the star formation lags behind the accretion of the gas involved, and the mass loss from stars ( $\mu$ ), the outflows from the galaxy ( $\eta_{out}$ ), and especially the recycling ( $\eta_{rec}$ ), all occur after the relevant events of star formation. The instantaneous quantities are sensible approximations once the system is indeed in or close to a quasi-steady state, and where the time delays are shorter than the timescale for long-term variations in quantities such as the accretion rate and the star-formation time.

In the simple version of the toy model addressed here, mass dependence enters only through the linear mass dependence of the accretion rate and the SFR (virial mass and gas mass respectively). The model ne-

glects any mass dependence of the specific accretion rate,  $t_{sf}$ , or  $\eta$ , as well as  $\mu$  (and  $p$ ). This is a reasonable approximation over a certain mass range, but it may fail outside this range. A mass dependence may have certain consequences, e.g., a suppressed sSFR in low-mass galaxies at high redshifts would tend to increase the amount of gas available for star formation at  $z \sim 2$  (e.g. Bouché et al. 2010; Krumholz & Dekel 2012). Introducing a mass dependence is possible, but it requires numerical integration of the bathtub model for a population of galaxies of different masses, and convolving the results with the mass function of galaxies. By integrating the continuity equations of the bathtub model one follows the time evolution of a given galaxy as it grows. This can be naturally compared to the average over observed galaxies selected at a fixed comoving number density at different redshifts, assumed to mimic the evolution of a given sample of galaxies, ignoring mergers. In the absence of mass dependence in the sAR,  $t_{sf}$  and  $\eta$ , the predictions can also be compared to galaxies selected to have the same mass at the different redshifts. Indeed, the observed sSFR evolution for samples of galaxies selected in those two different ways is rather similar (Salmon et al. 2014, Figure 17), indicating mass independence in the relevant mass range.

The stellar fraction in the accretion turned out to be a key factor. Given the uncertainty in this fraction, one may be tempted to try the extreme case where it is the same as the stellar fraction within the evolving galaxy at the same time,  $f_{sa} = f_s$ . This turns out to generate a rapid drop in  $f_g$  soon after the start of the integration, in sharp disagreement with observations. We learn that  $f_{sa}$  should grow much slower than  $f_s$ , consistent with the fact that a large fraction of the accreted baryons is associated with galaxies of much lower mass and with smooth accretion, including massive recycling. A more reliable estimate of  $f_{sa}$  at different epochs is yet to be determined.

The assumption that the SFR is proportional to the total gas mass is clearly a crude simplification, as we know that the SFR actually follows the molecular gas surface density, which does not necessarily follow the total gas mass density in the low-density and low SFR regime. Nevertheless, it is an approximation worth adopting even if crude, in the regime where it is not totally off, because it is the feature that drives the system into the self-regulated situation and makes it simple to work out.

We adopted above the most natural assumption that the depletion time  $t_{sf}$  is proportional to the disk dynamical time, and that the latter is proportional to the cosmological time. There is an observational indication for  $t_{sf} \propto (1+z)^{-1}$  out to beyond  $z \sim 2$  (Saintonge et al. 2013), which is not far from the  $t_{sf} \propto t$  assumed in the toy model. These observations are also consistent with the SFR being driven by the total gas mass. However, the assumption of  $t_{sf} \propto t$  may break down in different ways, e.g., the depletion time may vary in a slower pace, to the extreme that it may be close to constant in time in a certain epoch. At a given time, this would be like adopting a different SFR efficiency

$\epsilon$ , which would mostly affect the gas fraction  $f_g$ , but would have little effect on the sSFR and on  $f_{sv}$ .

The assumption that the outflow rate is proportional to the SFR with a constant mass-loading factor is supported by observations and is sensible theoretically for stellar feedback, but it is an approximation that may fail for AGN feedback and for other mechanisms that could be driving outflows. Our modeling of recycling as an instantaneous negative contribution to  $\eta$  is clearly simplified, and it may or may not capture the main features of the recycling process, which may be crucial for sorting out the discrepancy at  $z \sim 2$ .

The penetration parameter  $p$  is not a necessary ingredient of the toy model. It is required only for the comparison of the model with observational estimates that involve the total halo mass, such as  $f_{sv}$ . For a crude comparison with this observation, the typical value  $p \sim 0.5$  deduced from current simulations is appropriate, but a more detailed estimate of  $p$  from simulations that span a range of feedback strengths is desired.

## 7 CONCLUSION

The minimal bathtub toy model is shown to be a useful tool for tracing the roles played by key processes of galaxy evolution and identifying major successes and tentative failures in reproducing observations at high redshift. This model is based on simplified but robust continuity equations for the gas and for the stars. Because of the generic monotonic dependence of the SFR (and therefore outflow rate) on gas mass, the system is self-regulated into a unique asymptotic behavior, which can be approximated by a quasi-steady-state solution. The simple time and mass dependence of the average accretion rate into galaxies allows an approximate analytic quasi-steady state solution.

We derived the analytic QSS solution and evaluated the associated deviation from the exact solution for three observables: the sSFR, the gas fraction, and the stellar-to-virial mass fraction. We showed that the error is negligible for the first two, and is limited to the level of tens of percent for the third quantity. We studied the range of validity of the QSS solution, and found that the errors are smaller at later epochs, and when the outflows are stronger.

In the QSS regime, the average sSFR is proportional to the specific accretion rate, sAR, with an absolute value that is insensitive to the SFR efficiency in a dynamical time  $\epsilon$  and to the outflow mass-loading factor  $\eta$ . The gas fraction is determined by  $\epsilon$ , and  $f_{sv}$  is driven by  $\eta$ .

At high redshifts, where the accretion is assumed to consist of gas only, the simple toy model reproduces the observations rather well with no need for fine tuning. The specific SFR is predicted with no free parameters to be  $\text{sSFR} \simeq [(1+z)/3]^{5/2} \text{Gyr}^{-1}$ , slightly higher than the cosmological sAR, in general agreement with the rather noisy observed sSFR at  $z = 3 - 8$ . The observed gas fraction constrains the SFR efficiency in a

dynamical time to  $\epsilon \simeq 0.02$ . The low  $f_{sv}$  indicated from observations requires an outflow mass-loading factor of  $\eta \simeq 1 - 3$ , for a penetration efficiency of fresh gas into the galaxy of  $p = 0.5 - 1$  respectively. Thus, the main features of galaxy evolution at high redshifts are captured by the simplest toy model.

However, at  $z \sim 2$ , where stars are also accreted, through mergers, there is a difficulty in matching the observations. The model with the highest possible sSFR, where the outflows are fully recycled, falls short by a factor  $\sim 3$  compared to the observed sSFR, and it overestimates  $f_{sv}$ . With  $\eta \sim 3$ , the model reproduces the latter but underestimates the sSFR by an order of magnitude. Thus, the toy model points at a robust challenge to theory at  $z \sim 2$ .

A potential way to ease the tension at  $z \sim 2$  is by massive recycling, as in the case modeled by  $\eta = 0$  in the minimal bathtub model. A more sophisticated implementation of recycling in the model may be required for a better match. The missing population of quenched galaxies in the observed average sSFR hints at an additional promising remedy. The galaxies where  $\eta$  or  $f_{sa}$  are higher than average drive the predicted average sSFR down, and the same galaxies are indeed likely to be quenched in reality. Once these are removed, the predicted sSFR would become higher by a factor of 2-3 and thus closer to the observed value. Finally, the discrepancy at  $z \sim 2$  may be due to a breakdown of the QSS solution, e.g., by strong fluctuations in the accretion rate. Alternatively, one could not deny the possibility of some fundamental flaw in the assumptions that lie at the basis of the bathtub toy model. Identifying such a flaw would be very interesting.

One should conclude with a reminder that the bathtub toy model, at least in its trivial form discussed here, is not meant to provide a detailed model that perfectly matches the observations. It is useful for a simple and crude qualitative study of the central elements of galaxy evolution, and for pointing out robust successes or major potential failures in reproducing certain observations, which should trigger a more detailed study of these issues. This has been demonstrated here by showing the robust match to observations at  $z = 3 - 8$ , and by pointing out the non-trivial discrepancy at  $z \sim 2$ .

On the other hand, the bathtub toy model can be extended to address other major observables, such as the evolution of gas metallicity in and outside galaxies and the scaling relations involving metallicity, as well as the hot gas content in the circum-galactic medium filling the halo and the associated with hot-mode accretion into the galaxy. Such extensions can be found, e.g., in Krumholz & Dekel (2012), Davé, Finlator & Oppenheimer (2012), and Lilly et al. (2013), and they are shown to be good approximations (Pipino et al. 2014, in preparation).

## ACKNOWLEDGMENTS

This research has been supported by ISF grant 24/12, by GIF grant G-1052-104.7/2009, by a DIP grant, by

NSF grant AST-1010033, and by the I-CORE Program of the PBC and the ISF grant 1829/12.

## REFERENCES

- Behroozi P. S., Wechsler R. H., Conroy C., 2013, *ApJ*, 762, L31
- Bernardi M., Meert A., Sheth R. K., Vikram V., Huertas-Company M., Mei S., Shankar F., 2013, *MNRAS*, 436, 697
- Birrer S., Lilly S., Amara A., Paranjape A., Refregier A., 2014, arXiv:1401.3162
- Bouché N. et al., 2010, *ApJ*, 718, 1001
- Cacciato M., Dekel A., Genel S., 2012, *MNRAS*, 421, 818
- Daddi E. et al., 2010a, *ApJ*, 713, 686
- Daddi E., Dickinson M., Morrison G., Chary R., Cimatti A., Elbaz D., Frayer D., et al., 2007, *ApJ*, 670, 156
- Daddi E. et al., 2010b, *ApJ*, 714, L118
- Davé R., 2008, *MNRAS*, 385, 147
- Davé R., Finlator K., Oppenheimer B. D., 2012, *MNRAS*, 421, 98
- Davé R., Oppenheimer B. D., Finlator K., 2011, *MNRAS*, 415, 11
- Dekel A., Birnboim Y., 2006, *MNRAS*, 368, 2
- Dekel A., Bournaud F., Mandelker N., 2014, arXiv:1310.1074
- Dekel A., Burkert A., 2014, arXiv:1310.1074
- Dekel A., Krumholz M. R., 2013, *MNRAS*, 432, 455
- Dekel A., Sari R., Ceverino D., 2009, *ApJ*, 703, 785
- Dekel A., Zolotov A., Tweed D., Cacciato M., Ceverino D., Primack J. R., 2013, *MNRAS*, 435, 999
- Duncan K., onselice C. J., Mortlock A., et al., 2014, arXiv:1400.0000
- Fakhouri O., Ma C.-P., 2008, *MNRAS*, 386, 577
- Forbes J. C., Krumholz M. R., Burkert A., Dekel A., 2013, arXiv:1305.2925
- Genel S., Bouché N., Naab T., Sternberg A., Genzel R., 2010, *ApJ*, 719, 229
- Genel S., Dekel A., Cacciato M., 2012, *MNRAS*, 425, 788
- Genel S. et al., 2008, *ApJ*, 688, 789
- Genzel R. et al., 2008, *ApJ*, 687, 59
- Genzel R., Newman S., Jones T., Förster Schreiber N. M., Shapiro K., Genel S., Lilly S. J., et al., 2011, *ApJ*, 733, 101
- Genzel R., Tacconi L. J., Gracia-Carpio J., Sternberg A., Cooper M. C., Shapiro K., Bolatto A., et al., 2010, *MNRAS*, 407, 2091
- Gonzalez V., Bouwens R., Illingworth G., Labbe I., Oesch P., Franx M., Magee D., 2012, arXiv:1208.4362
- González V., Labbé I., Bouwens R. J., Illingworth G., Franx M., Kriek M., Brammer G. B., 2010, *ApJ*, 713, 115
- Guo Q., White S., Li C., Boylan-Kolchin M., 2010, *MNRAS*, 404, 1111
- Kennicutt R. C., 1989, *ApJ*, 344, 685
- Kravtsov A., Vikhlinin A., Meshcheryakov A., 2014, arXiv:1401.7329
- Kriek M. et al., 2006, *ApJ*, 649, L71
- Krumholz M. R., Dekel A., 2012, *ApJ*, 753, 16
- Krumholz M. R., Dekel A., McKee C. F., 2012, *ApJ*, 745, 69
- Krumholz M. R., Tan J. C., 2007, *ApJ*, 654, 304
- Krumholz M. R., Thompson T. A., 2007, *ApJ*, 669, 289
- Labbé I., González V., Bouwens R. J., Illingworth G. D., Franx M., Trenti M., Oesch P. A., et al., 2010, *ApJ*, 716, L103
- Labbé I., Oesch P. A., Bouwens R. J., Illingworth G. D., Magee D., González V., Carollo C. M., et al., 2013, *ApJ*, 777, L19
- Lilly S. J., Carollo C. M., Pipino A., Renzini A., Peng Y., 2013, *ApJ*, 772, 119
- Moster B. P., Naab T., White S. D. M., 2013, *MNRAS*, 428, 3121
- Moster B. P., Somerville R. S., Maulbetsch C., van den Bosch F. C., Macciò A. V., Naab T., Oser L., 2010, *ApJ*, 710, 903
- Narayanan D., Bothwell M., Davé R., 2012, *MNRAS*, 426, 1178
- Neistein E., Dekel A., 2008, *MNRAS*, 388, 1792
- Neistein E., van den Bosch F. C., Dekel A., 2006, *MNRAS*, 372, 933
- Reddy N. A., Pettini M., Steidel C. C., Shapley A. E., Erb D. K., Law D. R., 2012, *ApJ*, 754, 25
- Saintonge A., Lutz D., Genzel R., Magnelli B., Nordon R., Tacconi L. J., Baker A. J., et al., 2013, *ApJ*, 778, 2
- Salmon B., Papovich C., Finkelstein S. L., et al., 2014, arXiv:1400.0000
- Stark D. P., Ellis R. S., Bunker A., Bundy K., Targett T., Benson A., Lacy M., 2009, *ApJ*, 697, 1493
- Stark D. P., Schenker M. A., Ellis R., Robertson B., McLure R., Dunlop J., 2013, *ApJ*, 763, 129
- Steidel C. C., Erb D. K., Shapley A. E., Pettini M., Reddy N., Bogosavljević M., Rudie G. C., Rakic O., 2010, *ApJ*, 717, 289
- Tacconi L. J. et al., 2010, *Nature*, 463, 781
- Tacconi L. J., Neri R., Genzel R., Combes F., Bolatto A., Cooper M. C., Wuyts S., et al., 2013, *ApJ*, 768, 74
- Tal T., Dekel A., Oesch P., et al., 2014, arXiv:1312.0000
- Tinsley B. M., 1980, *Fund. Cosmic Phys.*, 5, 287
- van de Voort F., Schaye J., Booth C. M., Dalla Vecchia C., 2011, *MNRAS*, 415, 2782
- van Dokkum P. G. et al., 2008, *ApJ*, 677, L5
- Weinmann S. M., Neistein E., Dekel A., 2011, *MNRAS*, 417, 2737
- Whitaker K. E., van Dokkum P. G., Brammer G., Franx M., 2012, *ApJ*, 754, L29
- Woo J., Dekel A., Faber S. M., et al., 2013, *MNRAS*, 428, 3306